# Selective Observation and Quantification of Amorphous Trans Conformers in Doubly $^{13}$C-Labeled Poly(ethylene terephthalate), PET, by Zero-Quantum Magic-Angle-Spinning Solid-State NMR

**Hironori Kaji*,‡ and Klaus Schmidt-Rohr†**

*Department of Chemistry and Ames Laboratory, Iowa State University, Ames, Iowa 50011, and Institute for Chemical Research, Kyoto University, Uji, Kyoto, 611-0011, Japan*

*Received February 15, 2002*

ABSTRACT: A new method for identifying and quantifying conformations of $^{13}$C-labeled polymer segments in magic-angle spinning (MAS) nuclear magnetic resonance (NMR) spectra is introduced. The observed magnetization is dephased by the difference of the recoupled anisotropic chemical shifts, reflecting relative orientation, of two sites with a significant $^{13}$C−$^{13}$C dipolar interaction. Signals of trans conformations decay more slowly than those near gauche or cis if the chemical-shift tensors in the trans conformation are related by inversion symmetry. This permits an estimate of the trans:gauche ratio. The experiments, which are based on zero-quantum (ZQ) or double-quantum/single-quantum (DQ-2SQ) dephasing under the recoupled chemical-shift anisotropy (CSA), yield selective MAS spectra of methylene groups in trans or gauche conformations. For the O−$CH_2$−$CH_2$−O moieties in amorphous and semicrystalline poly(ethylene terephthalate) (PET), the ZQ-CSA-dephasing and (DQ-2SQ)-CSA-dephasing methods enable selective observation of the amorphous trans components, which cannot be detected by traditional CP/MAS experiments due to complete overlap with dominant gauche and crystalline trans signals. The observed amorphous trans chemical shift is close to that in PET crystallites; it cannot be rationalized based on the empirical $\gamma$-gauche effect. These experiments also provide signal decay curves from which torsion angles can be determined, with high angular resolution around the trans state. The data yield 12 ± 3% trans in amorphous PET, with a approximate 16° standard deviation of the torsion angles from the ideal trans state. In semicrystalline PET, the total trans fraction is 43 ± 3% and the best estimate of the crystalline-trans fraction, which corresponds to the degree of crystallinity, is 23 ± 5%; the amorphous trans fraction is 20 ± 5%. The trans fraction in the amorphous regions of semicrystalline PET, 26 ± 5%, is significantly higher than the 12 ± 3% in amorphous PET. The experiment is easily combined with double-quantum spectroscopy of isotropic chemical shifts, which provides further information on the isotropic chemical shifts of specific conformers. In amorphous PET, the two $CH_2$ groups in trans conformers are found to experience similar local fields.

## 1. Introduction

The elucidation of the microscopic structure of solid polymers is an important goal in polymer science since the establishment of structure−property relationships is crucial for the design of improved or novel materials. Solid-state nuclear magnetic resonance (NMR) is one of the most versatile and promising methods for characterizing the structure of disordered polymers in detail.[1−4] A particularly important and easily accessible observation in magic-angle spinning (MAS) NMR spectra is the isotropic chemical shift. Therefore, it has been extensively used for the analysis of segmental conformations in synthetic[5,6] and biopolymers.[7−10] For example, conformations in hydrocarbon chains are analyzed based on the $\gamma$-gauche effect, an upfield shift by ~4 ppm for each $\gamma$-substituent in a gauche bond.[5,11] However, this shift is empirical, and packing effects can lead to shifts of a comparable magnitude.[12,13]

In this paper, we present new NMR techniques for analyzing local conformations in $^{13}$C-labeled solid materials under MAS. The angle between two nearby $^{13}$C-labeled sites is quantitatively analyzed via the relative orientation of their chemical-shift tensors, which determines the modulation of the resonance lines in the MAS spectrum. When the sites are separated by one or two bonds, information on the torsion angle(s) of the bond(s) is obtained (see Figure 1). In particular, trans conformations between $CH_2$ groups are often characterized by a very slow intensity decay. Thus, the MAS signals of these trans conformations can be selected, which may be useful for deconvolution of $^{13}$C MAS spectra of the same polymer without isotopic labeling. Zero-quantum[14] (ZQ) or combined double-quantum/single-quantum (DQ-2SQ) filtering is an important aspect of this approach. It removes the signals of isolated $^{13}$C spins so that exclusively the desired spin pair signals are obtained at short ZQ (or DQ) excitation times. The (DQ-2SQ) version is easily combined with two-dimensional (2D) DQ spectroscopy of isotropic chemical shifts (solid-state INADEQUATE NMR)[15] that permits further characterization of the trans segments. The experiments are demonstrated on polyethylene (PE) and amorphous as well as semicrystalline poly(ethylene terephthalate), PET, containing $^{13}CH_2$−$^{13}CH_2$ spin pairs.

## 2. Experimental Section

**2.1. Samples.** Three samples were used in this work. (1) A melt-crystallized high-density PE sample labeled with dilute $^{13}CH_2$−$^{13}CH_2$ spin pairs. The ratio of directly bonded and isolated $^{13}$C nuclei is 4.4:1.1. A small amount of $^{13}CH_3$-labeled DL-alanine was added, providing a clear, resolved signal of isolated $^{13}$C spins near 21 ppm that permits easy assessment of the quality of the spin pair selection by the new ZQ and DQ pulse sequences. (2) A melt-crystallized PET (cPET)

* To whom correspondence should be addressed. E-mail: kaji@scl.kyoto-u.ac.jp.
† Iowa State University.
‡ Kyoto University.

10.1021/ma020246j CCC: $22.00 
Published on Web 09/14/2002

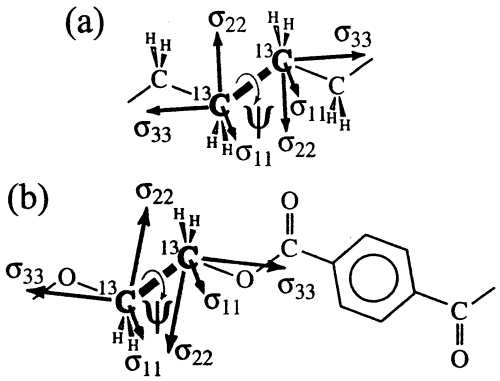


**Figure 1.** Schematic representations of the chemical-shift tensor orientations and the torsion angles $\psi$ for relevant $^{13}CH_2-^{13}CH_2$ spin pairs in (a) PE and (b) PET. For simplicity, planar all trans conformations with $\psi = 180°$ are shown for both polymers. The relative orientations of the segment-fixed chemical-shift tensors, and thus the torsion angles, can be characterized by the new "ZQ-CSA-dephasing" or "(DQ-2SQ)-CSA-dephasing" experiments. The polar coordinates of the $^{13}C-^{13}C$ bond in the chemical-shift principal-axes system (PAS) are $(\alpha, \beta) = (90°, 146.5°)$, (40°, 113°), and (90°, 126°) for trans conformers in PE,[19] trans conformers in PET,[1] and gauche conformers in PET,[1] respectively. In the conformation shown, the anisotropic $^{13}C$ chemical shifts of both $CH_2$ groups in the segment would be equal.

sample with $^{13}CH_2-^{13}CH_2$ spin pairs. Wide-angle X-ray scattering (WAXS) of the annealed sample shows significant crystallinity (estimated between 15 and 40%). DSC yields a crystallinity of 32 ± 4%; this includes 2% of a component melting already at 150 °C and the main (30%) melting peak at 242 °C. MAS $^{13}C$ NMR shows a clear crystalline peak and after $^{13}C$ $T_1$-filtering yields a predominantly crystalline signal. A deconvolution of the $^{13}C$ spectrum on this basis yields an estimated crystallinity of 28 ± 5% (26 ± 6% after correction for differential $T_{1\rho}$ relaxation of crystalline and amorphous signals during cross polarization (CP)). The material was not suitable for density measurements. (3) The same $^{13}CH_2$-labeled PET sample was quenched from the melt into ice−water to make the amorphous doubly $^{13}CH_2$-labeled PET (aPET). The melt was held at 280 °C for 10 min in a metal die of 4-mm diameter and 1-mm thickness. Kapton was used as a mold release. The density of the quenched disks, measured in a gradient column, is 1.340 g/cm$^3$. Assuming amorphous and crystalline densities of $\rho_A = 1.336$ g/cm$^3$ and $\rho_C = 1.510$ g/cm$^3$, respectively, the residual crystallinity is estimated as 2%.

**2.2. NMR Parameters.** Experiments were performed at 100 MHz for $^{13}C$ in a 4-mm MAS probehead on a Bruker DSX-400 spectrometer at 293 K and at a spinning speed, $\omega_r$, of 12 kHz. The sample amounts are as small as ∼10 mg for all the NMR experiments. The $^{13}C$ 360° pulse length during the HORROR nutation was 162.7 $\mu$s, which is slightly shorter than 2/12 kHz to account for some additional small delays. The contact time for CP was 0.5 ms. The acquisition time, dwell time, and recycle delay were 16 ms, 12 $\mu$s, and 5 s, respectively. $^1H$ and $^{13}C$ 90° pulse lengths were 4.0 and 6.0 $\mu$s, respectively. The relatively weak $^{13}C$ radio frequency (rf) field strength of $\gamma B_1/2\pi = 42$ kHz permits achievement of a larger ratio of proton-to-carbon rf field strengths, which minimizes $^1H-^{13}C$ dipolar recoupling.[16] Due to the small chemical-shift anisotropy and isotropic-shift differences of the $OCH_2$ carbons of PET, the weaker $^{13}C$ pulse strength does not entail excitation problems. The $^1H$ decoupling during MQ excitation, reconversion, and evolution was $\gamma B_1/2\pi = 87$ kHz. During $^{13}C$ pulses, a stronger $^1H$ decoupling field of 98 kHz was applied to minimize $^1H-^{13}C$ dipolar recoupling. Two-pulse phase-modulation (TPPM) $^1H$ decoupling[17] with a field strength of 65 kHz and an optimum $^1H$ pulse length of 7.6 $\mu$s was applied during acquisition. For solid-state INADEQUATE experiments, the $^{13}C$ frequency was switched by 1.5 kHz from the on-resonance frequency during the evolution time[3] so that ZQ and single-quantum (SQ) artifacts can be separated from the relevant DQ signals.

## 3. Description of NMR Pulse Sequences

**3.1. Principle of NMR Torsion-Angle Measurements.** On the basis of the dependence of the chemical-shift frequency $\omega$ on the orientation of the segment relative to the external magnetic field,[18] suitably designed solid-state NMR experiments can measure the relative orientation of two nearby $^{13}C$-labeled segments.[19] In $^{13}CH_2-^{13}CH_2$ moieties, this provides information on the torsion angle. "Nearby" means that a significant dipolar coupling between the $^{13}C$ nuclear magnets $S$ and $L$ exists that permits transfer of spin coherence between them. In this work, we focus on methods that detect modulations of the signal by the *difference* in the anisotropic chemical shifts, $\omega_S - \omega_L$. When the segments are parallel or related by inversion symmetry, as in $CH_2$ groups in the trans conformation (as shown in Figure 1), the modulation or signal decay vanishes, which is particularly easy to detect.

Under magic-angle spinning, the chemical-shift anisotropy (CSA) frequency varies due to the sample-rotation-induced changes in segmental orientation. Therefore, in the following, we express the frequency effects in terms of the phase $\Phi$ of the magnetization, which in simple cases is the time integral of the frequency $\omega$. Thus, the signal modulation by the difference frequency $\omega_S - \omega_L$ is expressed in terms of the phase difference $\Phi_S - \Phi_L$. When $\omega_S - \omega_L = 0$ due to parallel chemical-shift tensor orientation, $\Phi_S - \Phi_L = 0$ also, and again no signal decay occurs (see Figure 3 or 8a below). For non-trans conformers, $\Phi_S - \Phi_L \neq 0$, which results in signal decay that reflects the torsion angle.

**3.2. NMR Background: MQ Coherences and Recoupling.** Our new NMR methods use the concept of multiple-quantum (MQ) coherences, specifically zero-quantum (ZQ) and double-quantum (DQ) coherences, to generate modulation by $\Phi_S - \Phi_L$. In our system, these MQ coherences represent spin states of two $^{13}C$ spins that evolve with the difference (ZQ) or sum (DQ) of the chemical shifts of the two spins.[20] By the same token, nuclear magnetization, which evolves with the chemical-shift frequency of a single spin, is an example of single-quantum (SQ) coherence.

ZQ or DQ coherences can be generated from magnetization by a period of evolution under the dipolar coupling between the two nuclear magnets, followed by a radio frequency pulse. The dipolar evolution generates a (single-quantum) two-spin coherence, which the pulse of suitable phase and duration converts into ZQ or DQ coherence or, more typically, a mix of the two. An efficient notation for analyzing the spin dynamics quantitatively is provided by the product-operator formalism;[18,20] see the Appendix.

After evolution of the ZQ or DQ coherence with the difference or sum chemical-shift frequency, respectively, a pulse and another period of dipolar coupling convert the undetectable ZQ or DQ coherence back into observable magnetization. The behavior of the ZQ or DQ coherence is detected indirectly through modulation of the observable magnetization. Specific schemes of cycling the phases of the radio frequency pulses enable selective observation of the modulation due to the ZQ or due to the DQ coherence evolution.[20] Since ZQ or DQ coherences cannot exist for isolated $^{13}C$ spins, this phase

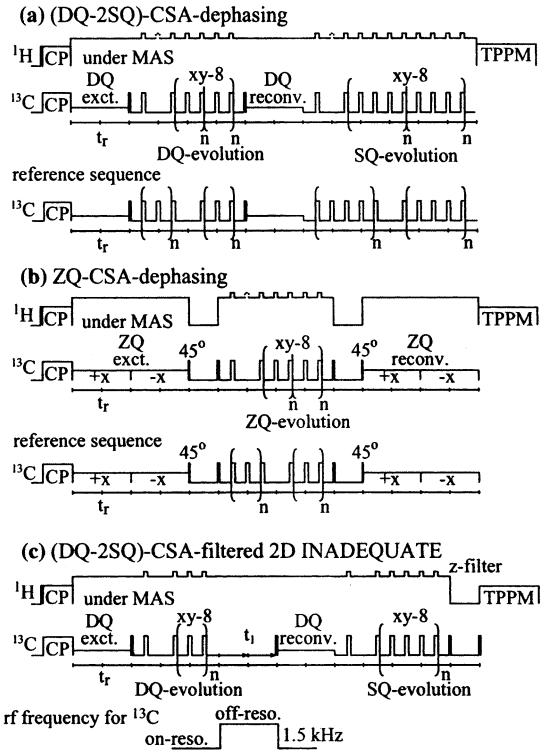


**Figure 2.** (a) (DQ-2SQ)-CSA-dephasing pulse sequence. (b) ZQ-CSA-dephasing pulse sequence. The reference pulse sequences, with the same total duration and number of pulses, are also shown for either experiment. (c) 2D solid-state INADEQUATE pulse sequence after a (DQ-2SQ)-CSA filter.

cycling automatically selects the signals of $^{13}C$ spin pairs.

The experiments are performed with magic-angle sample spinning (MAS), which removes line broadening by the chemical-shift anisotropy. MAS also averages weak dipolar couplings to zero over the course of complete sample rotation periods. But to generate the MQ coherences, we require dipolar evolution of significant duration. For this purpose, the dipolar coupling must be reintroduced during certain times in the pulse sequence. This can be achieved by applying rotation-synchronized radio frequency pulses, which interfere with the time averaging imposed by magic-angle spinning. This effect is known as "recoupling".[21] We use the HORROR recoupling method.[22]

**3.3. Overview over the Pulse Sequences.** The pulse sequences for the (DQ-2SQ)-CSA-dephasing and ZQ-CSA-dephasing experiments are shown in Figure 2. Cross polarization from $^{1}H$ generates $^{13}C$ magnetization. The subsequent DQ or ZQ excitation selects $^{13}C-^{13}C$ spins pairs and removes the signal of isolated $^{13}C$ spins, as demonstrated by the spectra in Figure 3.

As shown below, the DQ evolution compensated by SQ evolution with doubled duration, or the ZQ evolution, creates the desired $\langle \exp(i(\Phi_S - \Phi_L))\rangle$ modulation. To prevent their averaging by MAS, the anisotropic chemical shifts are recoupled by a train of 180° pulses during ZQ or DQ evolution. At the same time, the isotropic chemical shifts are refocused. For generating and later reconverting MQ coherence under MAS, we recouple the $^{13}C-^{13}C$ dipolar interaction using the HORROR scheme,[22] which is suitable for $^{13}CH_2$ groups with strong C−H dipolar couplings but with narrow CSA widths and small isotropic-shift differences. Note that (POST)C7[23,24] or MELODRAMA[25] schemes are more suitable for $^{13}C$ sites with large CSA widths. The excitation and the reconversion modulate the coherence by $\sin^2(\phi_{SL})$, where $\phi_{SL}$ is the phase acquired under the recoupled $S-L$ dipolar coupling.

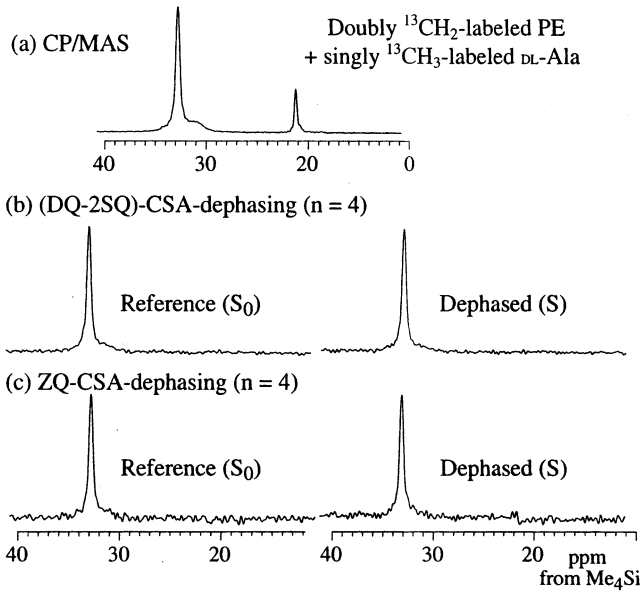


**Figure 3.** 1D MAS spectra of a mixture of doubly $^{13}CH_2$-labeled PE and singly $^{13}CH_3$-labeled DL-Ala at 293 K. (a) CP/MAS spectrum. (b) Right: (DQ-2SQ)-CSA-dephased spectrum at $n = 4$. Left: reference spectrum. 512 scans were acquired for each spectrum. (c) Right: ZQ-CSA-dephased spectrum at $n = 4$. Left: reference spectrum. 64 scans were acquired for each spectrum. Spinning speed: 12 kHz.

In the following, we give brief verbal descriptions of our three newly developed pulse sequences, focusing on the torsion-angle-dependent modulation of the signal by the difference of the chemical-shift anisotropies. The detailed quantum-mechanical calculations are described in the Appendix.

**3.4. (DQ-2SQ) Sequence.** In the pulse sequence at the top of Figure 2a, a DQ coherence is generated and selected by 90° pulses of suitable phases. During the DQ period of duration $2nt_r$, the coherence evolves under the sum chemical shift, acquiring a phase $\Phi_S + \Phi_L$. In alternate scans, the $\cos(\Phi_S + \Phi_L)$- and $\sin(\Phi_S + \Phi_L)$-modulated components of the DQ coherence, selected by suitable $j$*45°-shifted pulses, are reconverted into observable magnetization of $S$ and $L$. In the SQ period of duration $4nt_r$ the magnetization of the spin $S$ acquires a phase $2\Phi_S$ and that of $L$ a phase $2\Phi_L$. As a result, the finally detected signal of the $S$ spin is modulated both by $\sin^2 \phi_{SL}$ and by

$$\langle[\cos(\Phi_S + \Phi_L) - i \sin(\Phi_S + \Phi_L)] \exp(i2\Phi_S)\rangle = \langle \exp(-i(\Phi_S + \Phi_L)) \exp(i2\Phi_S)\rangle = \langle \exp(i(\Phi_S - \Phi_L))\rangle \quad (1)$$

The real part for the $L$-spin signal is the same as in eq 1. The pointed brackets indicate the average over all segmental orientations. Apart from the $\sin^2 \phi_{SL}$ modulation (not written explicitly), eq 1 is formally identical to the corresponding Center-band Only Detection of EXchange (CODEX) modulation[26,27] and can be simulated accordingly.

At the bottom of Figure 2a, the pulse sequence for the reference signal $S_0$ is shown. It has the same number of pulses and delays, but in both the DQ and the SQ evolution period, one 180° pulse is moved so that

the recoupling effect is removed by sign cancellation of corresponding periods.[21]

**3.5. ZQ Version.** A modulation of $\langle\exp(i(\Phi_S - \Phi_L))\rangle$ as in eq 1 is typical of ZQ evolution, which depends on the chemical-shift difference.[14] A ZQ coherence acquires this modulation within a time $2nt_r$, without the lengthy $4nt_r$ SQ evolution; this is a practical advantage. On the other hand, ZQ excitation is $1/2^{1/2}$ times less efficient than DQ generation (see the Appendix for details). Figure 2b displays a pulse sequence for generating the ZQ coherence in close analogy to the (DQ-2SQ) pulse sequence discussed above.

**3.6. (DQ-2SQ)-Filtration of 2D "INADEQUATE" Spectra.** In the (DQ-2SQ) experiment, double-quantum isotropic-chemical-shift evolution can be achieved quite conveniently by incorporating an incremented $t_1$-period of free isotropic-shift evolution into the DQ period as shown in Figure 2c. The corresponding phase $(\omega_{iso,S} + \omega_{iso,L})t_1$ adds to the DQ phase, which is thus $\Phi_{S,tot} + \Phi_{L,tot} = \Phi_S + \Phi_L + (\omega_{iso,S} + \omega_{iso,L})t_1$, where $t_1$ is an integer number of rotation periods. Since $\exp\{i(\omega_{iso,S} + \omega_{iso,L})t_1\}$ is unaffected by the orientational averaging, we can separate the isotropic evolution and "DQ-2SQ" modulation factors:

$$\begin{aligned}&\langle\exp(-i(\Phi_{S,tot} + \Phi_{L,tot}))\exp(i2\Phi_S)\rangle\\ &= \langle\exp\{-i(\Phi_S + \Phi_L + (\omega_{iso,S} + \omega_{iso,L})t_1)\exp(i2\Phi_S)\rangle\\ &= \exp(-i(\omega_{iso,S} + \omega_{iso,L})t_1)\langle\exp(i(\Phi_S - \Phi_L))\rangle \quad (2)\end{aligned}$$

Pure-phase 2D spectra were obtained by storing cosine and sine components separately before detection, generating a regular amplitude modulation.

## 4. Results and Discussion

**4.1. ZQ and (DQ-2SQ) Experiments on PE.** In Figure 3a, a standard CP/MAS spectrum of a mixture of doubly $^{13}CH_2$-labeled PE and singly $^{13}CH_3$-labeled DL-Ala is displayed. For the same sample, Figure 3b shows a MAS spectrum acquired after (DQ-2SQ)-CSA-dephasing (right) and its reference spectrum (left) with $n = 4$, that is, $4t_r$ of DQ and $8t_r$ of SQ evolution under CSA recoupling. Corresponding spectra after ZQ-CSA-dephasing are shown in Figure 3c. Compared with the CP/MAS spectrum in Figure 3a, the signal of the isolated $^{13}CH_3$ carbons of DL-Ala is suppressed in both DQ and ZQ experiments, indicating that the DQ (or ZQ) filter selects the $^{13}C$ spin pairs cleanly. The integral intensities of the PE signals in the (DQ-2SQ)- and ZQ-CSA-dephasing spectra, $S$, are the same as those of the corresponding reference spectra, $S_0$. These results indicate that $\Phi_S - \Phi_L = 0$ for all pairs of segments (see eq 1), that is, that the orientation-dependent chemical shifts of the two $CH_2$ groups in the semicrystalline PE are identical. This is characteristic of the exact trans conformation, where the two $CH_2$ groups are related by inversion symmetry, which results in identical chemical shifts. The amorphous components in PE are suppressed due to their weak $^{13}C$ dipolar couplings.

Due to the long $T_2$ of semicrystalline PE under high-power $^1H$ decoupling, the signal-to-noise ratio in the ZQ version is by about $1/2^{1/2}$ smaller than that of the (DQ-2SQ) version, despite the 3 times shorter CSA recoupling period in the ZQ experiment. The number of scans was 8 times smaller for the ZQ experiments in Figure 3.

**4.2. Amorphous PET.** Figure 4a−c shows ZQ-CSA-dephased spectra of aPET with $n = 1$, 2, and 4, respectively, out of a series of $n = 0$, ..., 4. The respective reference spectra are shown at the top. The intensities at ca. 64 and 62 ppm are negative and positive, respectively, for the spectrum with $n = 2$. This indicates that these are signals of segments with very different torsion angles. The residual signal at 62 ppm in the ZQ-CSA-dephased spectrum with $n = 4$ (Figure 4c, bottom) prove the existence of trans conformers in aPET. It identifies their resonance position and shape convincingly for the first time. Note that the full CP/MAS spectrum does not show any significant feature attributable to the amorphous trans (aT) peak. The broader line shape compared to the crystalline trans (cT) peak in cPET identifies the trans components selected here clearly as noncrystalline, as shown in Figure 6. No sharp crystalline peak is detectable in the trans signal $S$ at $n = 4$. On that basis, we can safely estimate that cT conformers, if present, make up less than 1/6 of the trans fraction, that is, <2% of the total signal $S_0$ of this aPET sample. The maximum percentage of the crystalline component thus obtained is comparable to that from the density measurement.

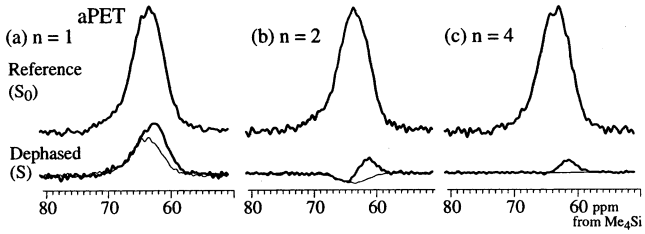


**Figure 4.** ZQ-CSA-dephased spectra of amorphous doubly $^{13}CH_2$-labeled PET (aPET) at 293 K at (a) $n = 1$, (b) $n = 2$, and (c) $n = 4$. Top: reference spectra. Bottom: ZQ-CSA-dephased spectra. Thin lines: Same pure-gauche $\Delta S$ $(=S_0 - S)$ spectrum for $n = 1$, with different scaling factors for deconvolution of the dephased spectra $S$ into gauche and trans signals. 256 scans were acquired for all the reference spectra and the dephased spectrum with $n = 1$. For the dephased spectra with $n = 2$ and 4, 1024 and 2048 scans were acquired and their intensities were scaled to $^1/_4$ and $^1/_8$, respectively. Spinning speed: 12 kHz.

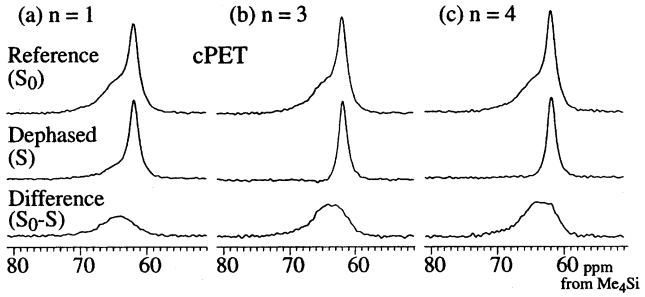


**Figure 5.** ZQ-CSA-dephased spectra of semicrystalline doubly $^{13}CH_2$-labeled PET (cPET) at 293 K at (a) $n = 1$, (b) $n = 3$, and (c) $n = 4$. Top: reference spectra $S_0$. Middle: ZQ-CSA-dephased spectra $S$. Bottom: difference spectra $\Delta S = S_0 - S$. For all the measured spectra, 384 scans were acquired. Spinning speed: 12 kHz.

**4.3. Semicrystalline PET.** Figure 5a−c shows ZQ-CSA-dephased spectra of cPET with $n = 1$, 3, and 4, respectively. The reference spectra, shown at the top, have almost the same line shape as the CP/MAS spectrum, indicating that differential $T_2$ relaxation during the experiment is a minor effect that can be taken into account in the quantitative analysis (see below). The spectra consist of a sharp line at about 62 ppm and a broad line distributed around 64 ppm. These resonance lines correspond to crystalline and amorphous components of PET as reported in refs 28 and 29. The

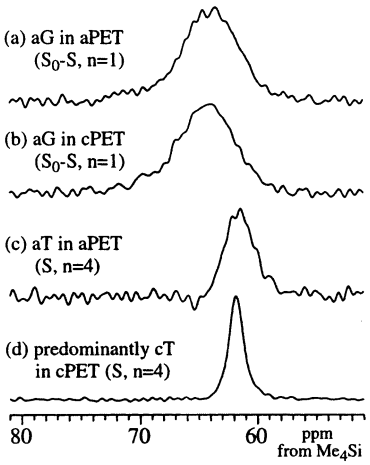


**Figure 6.** Selective conformer subspectra of aPET and cPET: (a) Pure amorphous gauche (aG) component in aPET: ZQ-CSA-dephasing difference spectrum $\Delta S = S_0 - S$ at $n = 1$. (b) Pure aG component in cPET: ZQ-CSA-dephasing difference spectrum $\Delta S$ at $n = 1$. (c) Amorphous trans (aT) component in aPET: ZQ-CSA-dephased spectrum $S$ at $n = 4$. (d) Pure trans component in cPET, which contains all the crystalline trans (cT) and approximately half of the aT components: ZQ-CSA-dephased spectrum of cPET at $n = 4$ (cT:aT = 0.73:0.27). The intensity of each spectrum is scaled to the same maximum peak height. Spinning speed: 12 kHz.

corresponding torsion angles can be estimated from the ZQ-CSA dephasing of the signal intensities as discussed below.

The ZQ-CSA dephasing of the gauche (amorphous gauche: aG) signal is much faster than that of the trans signals. Therefore, the gauche component is strongly decreased at $n = 1$ and negligible at $n = 3$ and 4 as shown in the middle row of Figure 5. A pure gauche spectrum can be obtained by subtracting the ZQ-CSA-dephased ($S$) spectrum for $n = 1$ from the reference ($S_0$) since the trans components are virtually completely retained in the $S$ spectrum. This pure-gauche spectrum is shown in the bottom row of Figure 5a. At $n = 3$ and 4, the difference spectrum, at the bottom of Figure 5b,c, also contains a significant fraction of the aT, but no cT since the $OCH_2-CH_2O$ moieties in the crystalline component are in the exact trans state and the chemical-shift tensors of the two bonded $^{13}C$ nuclei are parallel. The contribution from aT conformers is discussed below.

**4.4. Conformer-Selective MAS Spectra of PET.** Figure 6 compiles spectra specific to various conformers in cPET and aPET obtained by the ZQ-CSA-dephasing technique. The spectra of gauche conformers in aPET and cPET, shown in Figure 6a,b, are obtained selectively by subtracting the ZQ-CSA-dephased ($S$) spectrum for $n = 1$ from the reference ($S_0$). As mentioned above, at this short CSA recoupling time, only the magnetization of $^{13}CH_2$ pairs with greatly different anisotropic chemical shifts, that is, gauche or cis, is significantly dephased and shows up in the difference spectrum, while trans or transoid signals are virtually completely subtracted out. From these spectra, gauche line shapes in cPET and aPET are found to be identical.

The trans conformers are selectively observed (see Figure 6c,d) at sufficiently long dephasing times ($n > 2$) at which the intensity of the gauche signals has decayed to zero. The spectra confirm that the resonance width of an aT signal in Figure 6c is significantly larger than that of the predominantly cT signal in Figure 6d, which indicates that the intermolecular packing around

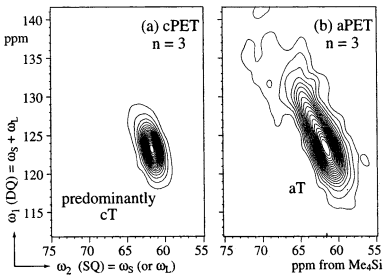


**Figure 7.** (DQ-2SQ)-CSA-filtered, 2D INADEQUATE spectra for (a) cPET and (b) aPET at 290 K at $n = 3$.

aT conformers is more disordered than that around crystalline segments, as expected.

**4.5. 2D INADEQUATE Spectra of Trans Components in PET.** The 2D INADEQUATE spectrum permits the correlated detection of the isotropic chemical shifts of the bonded $^{13}C$ sites. After (DQ-2SQ)-CSA-dephasing, the sites connected by trans bonds are selected. In an INADEQUATE spectrum, the frequency of one site is read off the $\omega_2$ dimension, the sum of the frequencies of the two sites along the $\omega_1$ dimension. In the spectrum of cPET shown in Figure 7a, the cT segments produce a single, relatively sharp peak on the diagonal of slope two in the spectrum since the frequencies of the bonded $^{13}C$ sites are the same.

In the amorphous sample, if all $^{13}C$ trans sites had the same probability to be bonded to any other site, a 2D Gaussian peak would result in the (sheared) 2D INADEQUATE spectrum. Instead, the spectrum of Figure 7b shows a pronounced ridge along the slope-two diagonal, indicating that the isotropic chemical shifts of the two trans-bonded $^{13}C$ sites are nearly the same. In other words, the two bonded sites experience the same local field, which might arise from packing or susceptibility effects.

**4.6. PET and the $\gamma$-Gauche Effect**. While in PE the $\gamma$-gauche effect produces a 2 ppm upfield shift of the amorphous segments relative to the crystalline peak, in PET, the aG signal is *downfield* from both the cT and the aT signals by ca. 2 ppm. This observed shift differences in PET cannot be explained based on the $\gamma$-gauche effect: Since the crystalline conformation is all trans, any gauche conformer in the noncrystalline regions should result in an upfield, not in a downfield, shift according to the $\gamma$-gauche analysis. The deviation might arise because the carbons in the $\gamma$-position from the $CH_2$ sites are carbonyl and aromatic carbons, while the $\gamma$-gauche effect is applicable mostly to aliphatic chains.

**4.7. Estimate of Torsion Angle in PE Crystallites.** In Figure 8, the normalized integral intensities, $S(n)/S_0(n)$, for the full $^{13}CH_2$ signal are plotted for PE, cPET, and aPET. For PE in Figure 8a, the normalized intensities are unity and independent of $2nt_r$. Figure 8a also displays simulated dephasing curves for various torsion angles. We find that torsion angles can be determined with high accuracy, especially near trans states. From the dephasing curves, the torsion angle for the crystalline component of PE is determined to be 180° ± 4°, confirming the exact trans state. Note that the angular resolution depends on the size of the CSA. With the same dephasing time and signal-to-noise ratio, a better resolution of ±2° could be attained for cPET, due to its larger chemical-shift anisotropy.

More precise angles between the chemical-shift tensor principal-axes systems could be determined by experiments with longer dephasing times or more scans.

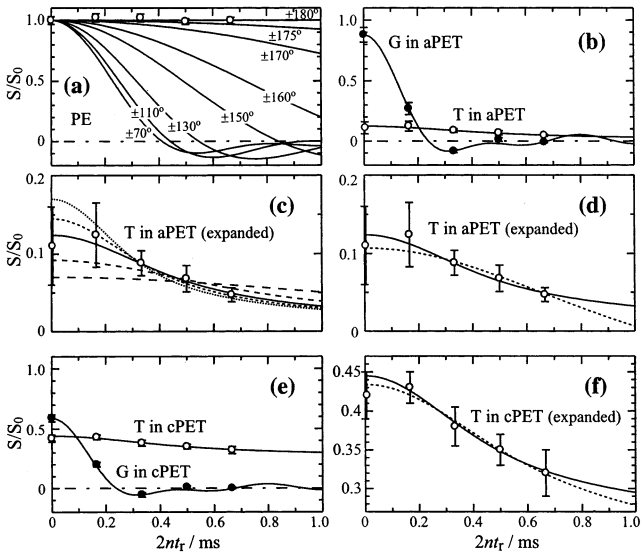


**Figure 8.** ZQ-CSA-dephasing curves as a function of $2nt_r$ for doubly $^{13}CH_2$-labeled PET and PE at 293 K. (a) Crystalline component of doubly $^{13}CH_2$-labeled PE (open circles). The torsion-angle dependence of dephasing curves for PE is also shown by solid lines. The consistency of the experimental data and their agreement with the simulated curve for a torsion angle of 180° confirms the reliability of the analysis. Higher angular resolution would be attained for the crystalline trans component of PET due to its larger CSA; the lines of ±175°, ±170°, ±160°, and ±130° for PE nearly correspond to ±178°, ±176°, ±171°, and ±160° for PET, respectively. (b) Dephasing curves for aPET. Gauche conformers, filled circles; trans conformers, open circles. Best-fit curves are also shown as solid curves, with gauche:trans = 0.88:0.12, corresponding to the minimum in the root-mean-square deviation in Figure 9b. The average torsion angle for gauche is 70° according to ref 1. The torsion angle for trans is distributed around 180° with a standard deviation $\sigma$ = 16°, under the assumption of a Gaussian distribution. (c),(d) Expanded data for trans conformers in (b). In (c), the simulated curves, shown by dashed and solid lines, have been calculated for different distribution widths, $\sigma$ = 5°, 10°, 16° (best-fit, solid line with $\chi^2$ = 0.258), 20°, and 25°, from the lower curve at $2nt_r = 0$. In (d), best-fit curves under the assumption of a single torsion angle (broken curve) and a distribution of torsion angles (solid curve) for aT are compared. The solid curve is the same as that in (c). The broken curve corresponds to the minimum in Figure 9a (gauche:trans = 0.89:0.11; torsion angle of 170°). (e) Data from cPET. Filled circles, gauche conformers; open circles, trans conformers. Best-fit curves are also shown as solid curves, with aG:aT:cT = 0.57:0.21:0.22, which gives a degree of crystallinity of 0.22. Note that all the fractions given here contain the $T_{1\rho}$ correction. In the simulation, the torsion angle of 180° and the average torsion angle of 70° are used for cT and aG conformers, respectively. The torsion angle for aT is distributed around 180° with a standard deviation, $\sigma$, of 16°, which is obtained from aPET. (f) Expanded data for trans conformers in (e). The solid line is the best-fit curve ($\chi^2$ = 0.796), with aT:cT = 0.49:0.51 (after $T_{1\rho}$ correction) with a torsion-angle distribution of width $\sigma$ = 16° for aT, corresponding to the minimum in Figure 9d. The simulated curve for aT:cT = 0.58:0.42 (after $T_{1\rho}$ correction) with a torsion-angle distribution width $\sigma$ = 12° for aT is also shown as a broken line, corresponding to the minimum in Figure 9c. For simulations, $\delta/2\pi$ = 20, 40, 41, and 31 (ppm) = 2, 4, 4.1, and 3.1 (kHz) are used for crystalline PE, cT in PET, aT in PET, and aG in PET, respectively.

However, in noncrystalline samples, the torsion angle in practice cannot be measured with such a high resolution since the orientation of the CSA principal-axes system in the molecular segment can vary by several degrees.

**4.8. Estimates of Torsion Angles and Conformer Fractions in aPET.** For aPET, much of the signal dephases quickly. The fast decaying fraction, which is due to the broad downfield peak, has been fit assuming gauche $O^{13}CH_2-{}^{13}CH_2O$ conformers with torsion angles near ±70° (see filled circles in Figure 8b). The simulated curves for torsion angles between 50° and 100° are actually indistinguishable, and the gauche torsion angle cannot be precisely determined in the present experiment. However, the decay curve does not conflict with our previously reported gauche torsion angle, 70° ± 9°, with a relatively narrow distribution,[1] obtained by 2D DOQSY without MAS, which is a superior NMR method for determining large torsion angles and their distributions.[1,3] The fit curve confirms that, at $n$ = 4, aG signals have been almost completely dephased and the residual intensity originates from aT conformers.

The aT signals are found also to have dephased significantly during this time. To estimate the aT fraction more reliably, the residual gauche signal at $n$ < 4 must be subtracted out. This is possible since the downfield slopes of the spectra are completely dominated by the gauche component. This subtraction requires suitable scaling of the pure-gauche spectrum of Figure 6a, as shown in the bottom row of Figure 4; fortunately, this procedure is quite insensitive to small uncertainties in the scaling factor since the gauche contributions to the dephased spectrum $S$ for $n$ > 1 are relatively small; see Figure 4b,c. In other words, each partially dephased spectrum is deconvoluted based on the experimentally determined pure gauche line shape, based on the wide pure-gauche region free of overlap from the trans component. The integral intensities of the residual aT conformers thus obtained are plotted as open circles in Figure 8b. Within the error bars associated with the deconvolution procedure, a smooth curve is obtained, corroborating the validity of the deconvolution. The amplitude of the curve at $n$ = 0, that is, without any dephasing, is 12 ± 3%. The pure gauche intensities also shown as filled circles in Figure 8b are obtained as part of the same procedure.

The best-fit parameters have been determined using a $\chi^2$ analysis. Figure 9a shows $\chi^2$ values as a function of the trans fraction and the trans torsion angle under the assumption of a single torsion angle for aT. The minimum deviation in Figure 9a is at a trans torsion angle of 170° and a trans fraction of 11%. Alternatively, in Figure 9b, $\chi^2$ values are calculated under the assumption of a Gaussian distribution of aT torsion angles around 180°. The minimum $\chi^2$ value is found for a standard deviation $\sigma$ = 16° for the torsion-angle distribution and a trans fraction of 12%. This is the best estimate of the trans content in this aPET sample. This value is within the previous reported values ranging from 5 to 24%.[30−35] Comparison of the best-fit curves obtained from these two analyses with the experimental data points is shown in Figure 8d.

**4.9. Estimates of Torsion Angles and Conformer Fractions in cPET.** For the quantitative data analysis of the cPET spectra, differential decays of crystalline- and amorphous-component signals, due to $T_{1\rho}$ relaxation during CP as well as $T_2$ decay during the pulse sequence, must be taken into account. In the following analysis, the differential-$T_{1\rho}$ factor of 0.88 and differential $T_2$ decays down to 0.82 have been corrected for quantitatively.[36,37] We carried out the quantitative analysis for torsion angles and conformer fractions in cPET in two complementary ways: based on residual intensities $S/S_0$, that is, dephasing curves, and based on the difference spectra $\Delta S$.

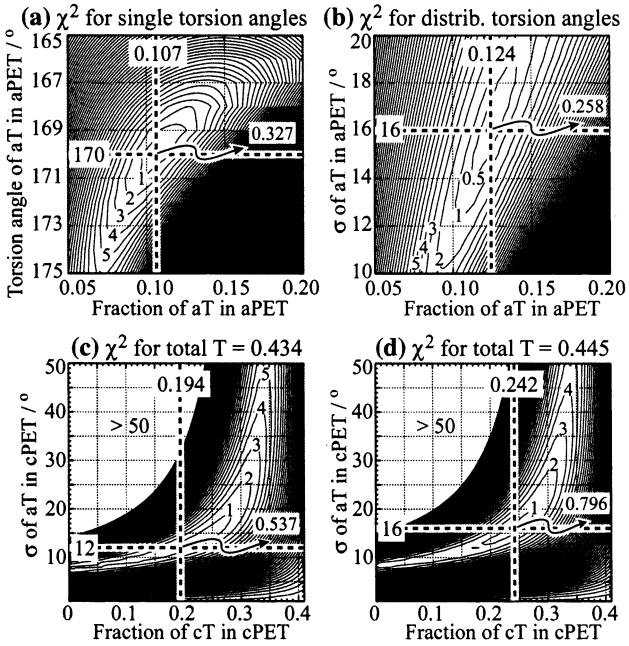


**Figure 9.** (a), (b) Normalized root-mean-square deviation ($\chi^2$) values between experimental and calculated decay curves for aT in aPET ((b), (c), or (d) in Figure 8). In (a), single torsion angles are assumed and the variables are the aT fraction and the aT torsion angle. The global minimum of $\chi^2$ yields an aT fraction of 0.107 and a torsion angle of 170°. In (b), Gaussian torsion-angle distributions centered at 180° are assumed and the variables are the aT fraction and the standard deviation of aT torsion angles, $\sigma$. An aT fraction of 0.124 and $\sigma$ = 16° are obtained from the global minimum of $\chi^2$. (c),(d) Values of $\chi^2$ between experimental and calculated decay curves for the total trans fraction in cPET ((e) or (f) in Figure 8). Note that composition fractions given here have not been corrected for $T_{1\rho}$ relaxation. Gaussian torsion-angle distributions centered at 180° are assumed for aT. There are three variables for (c) and (d): the total trans fraction, the cT fraction, and the torsion-angle distribution with $\sigma$ for aT. A parameter set with a total trans fraction = 0.434, cT fraction = 0.194, and $\sigma$ = 12° for aT gives the global minimum of $\chi^2$. In (c), $\chi^2$ values are calculated for a fixed total trans fraction of 0.434. Under the assumption that the $\sigma$ values for aT are the same (16°) in cPET and in aPET, the global minimum is obtained for a total trans fraction = 0.445 and cT fraction = 0.242. In (d), $\chi^2$ values are calculated for a fixed total trans fraction of 0.445.

**4.9.1. Quantitative Analyses Based on Dephasing Curves.** For cPET, a pure trans signal of intensity $S/S_0 = 0.32 \pm 0.03$ is obtained at $n = 4$ (before $T_{1\rho}$ correction). This represents a reliable lower limit for the total trans fraction and an upper limit for the crystallinity because it includes not only crystalline but also residual aT components. To determine the total trans content more accurately, and to separate the cT and aT fractions in this sample, the same deconvolution as described above was applied to each spectrum $S(n)$. The experimental pure gauche spectrum of cPET that was subtracted out has been shown in Figure 6b. Again, this procedure yields a smooth curve within the error margins (open circles in Figure 8e,f). It extrapolates to a total trans content of 43 ± 3% at $n = 0$ (after $T_{1\rho}$ correction). The time scale of the dephasing of the trans component roughly matches that of aT in aPET. The experimentally observed dephasing by 43−32% = 11% gives a lower limit for the aT fraction in the sample.

The quantitative least-squares analysis is illustrated in Figure 9c,d. The least-squares fitting of the trans dephasing curve in Figure 8e gives total trans and cT fractions of 0.434 and 0.194, respectively, and a torsion-angle distribution width of $\sigma$ = 12° under the assumption of Gaussian distribution of aT torsion angles around 180°. The $\chi^2$ values, with the total trans fraction fixed at 0.434 to reduce this to a two-dimensional search, are shown in Figure 9c. If we assume that the torsion-angle distribution of aT in cPET is the same as that in aPET ($\sigma$ = 16°), then the least-squares fitting procedure gives total trans and cT fractions of 0.445 and 0.242, respectively. The $\chi^2$ values with the total trans fraction fixed at 0.445 are shown in Figure 9d. The data can be fitted with an aT fraction of 20.3 ± 7% (21% ± 7% after $T_{1\rho}$ correction) and a degree of crystallinity of 24.2 ± 7% (22 ± 7%, after $T_{1\rho}$ correction). Note that the $\sigma$ widths of the aT distributions for cT > 0.30 (i.e., degrees of crystallinity >30%) are unreasonably large (>25°).

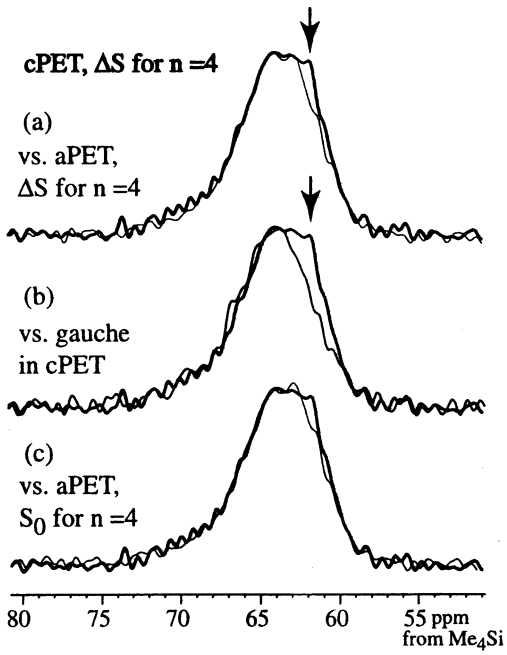


**Figure 10.** Comparison of the difference spectrum $\Delta S$ (=$S_0$ − $S$) of cPET at $n$ = 4 (thick lines) with three other spectra to clearly show the larger aT content in cPET relative to aPET. The $\Delta S$ at $n$ = 4 spectrum of cPET contains the aT that has dephased at $n$ = 4 and all the aG components in cPET. (a) Comparison with the difference spectrum $\Delta S$ of aPET at $n$ = 4, which contains the aT that has dephased at $n$ = 4, and all the aG components in aPET. (b) Comparison with the difference spectrum $\Delta S$ of cPET at $n$ = 1, which contains only aG signals. (c) Comparison with the spectrum $S_0$ of aPET at $n$ = 4, which contains all the aT and aG components in aPET. Note that direct comparison with the same $n$ values (i.e., (a) and (c)) intrinsically accounts for the differential $T_2$ decay. Spectra have been scaled to match the left, pure-gauche wing of the bands.

Of the noncrystalline components in cPET, the aT component makes up (21 ± 7%)/(1−0.22) = 27 ± 9% (18−36%). The trans content in aPET was found to be lower, 12 ± 3%.

**4.9.2. Quantitative Analysis Based on Spectral Comparison.** The significance of the increase in trans content of the noncrystalline component, relative to aPET, is confirmed by the spectra of Figure 10. They compare the difference signal $\Delta S$ of cPET at $n$ = 4 with three other spectra to estimate the trans fraction that has already been dephased at $n$ = 4. The comparison with the corresponding spectrum of aPET (Figure 10a) shows that the aT in the semicrystalline sample is different from that in aPET. It is either a larger fraction or more disordered; either factor would result in more dephasing.

The trans content in the $\Delta S(n = 4)$ spectrum of cPET can be determined by deconvolution with the pure-gauche spectrum of cPET (Figure 10b). The deconvolution yields a trans fraction of 14 ± 3% in the dephased spectrum $\Delta S$ at $n = 4$. This is confirmed by comparison with the undephased spectrum of aPET at the same $n = 4$ dephasing condition (Figure 10c); aPET was found to be 12 ± 3% trans. Since the $T_2$-corrected but $T_{1\rho}$-uncorrected total dephased signal, $\Delta S/S_0(n = 4) = 0.68$, is directly obtained from the experiments, the dephased trans fraction is 68% * 0.14 = 10 ± 3% of $S_0$. This is in good agreement with the dephasing of the trans fraction at $n = 4$ in Figure 8f, which was determined by the independent deconvolution procedure described above to be 43−32% = 11%. The advantage of the comparisons in Figure 10a,c is that they intrinsically account for differential $T_2$ decay. The averaged dephased aT fraction of 10.5 ± 3% at $n = 4$ is 0.5% lower than the value in the previous paragraph, resulting in a −1% correction of the aT fraction and a reduced error margin due to the two independent determinations, 20 ± 5%, and a 1% larger degree of crystallinity of 23 ± 5%.

**4.9.3. Amorphous Trans Fraction in cPET.** The analyses described above consistently yield a crystallinity of 23 ± 5%, an aT fraction of 20 ± 5%, and an aG fraction of 57% in cPET. These results suggest that the somewhat higher crystallinity obtained by DSC might include some of the imperfect trans conformers that are denoted as aT here. Another possibility is that recrystallization before melting occurs during DSC measurements. The degree of crystallinity from the ZQ-CSA dephasing experiments agrees satisfactorily with that obtained by $T_1$-filtered NMR.

Several authors assume that the aT component is related to some ordered region in the noncrystalline phase.[30,31,34,38−42] If this is true, the aT region must be more densely packed than the rest of the noncrystalline region.[41] According to Lin and Koenig,[34] the density of aT is 1.430 g/cm$^3$, which is intermediate between the densities of cT (1.510 g/cm$^3$) and pure gauche (1.326 g/cm$^3$) isomers. It must be noted, however, that for samples with a large aT fraction the degree of crystallinity calculated only from amorphous (1.336 g/cm$^3$) and crystalline (1.510 g/cm$^3$) densities would give slightly higher values than those calculated assuming three different density values.

**4.10. Angular Resolution.** The ZQ-CSA-dephasing experiment has high angular resolution for trans states, as indicated above. The cT signal does not give any observable decays and the torsion angle is determined to be 180° ± 4° for PE, that is, in the ideal trans state. In contrast, the aT signal in PET is dephased detectably, indicating that the aT conformers are not in the exact trans state but are distributed around or deviate from the ideal trans state. From the present experimental data, it is not reliably possible to determine whether the most probable conformation deviates from 180° or whether there is a torsion-angle distribution centered at 180°. However, in principle the ZQ (and DQ) techniques presented here have the potential to distinguish these two cases. Figure 8d shows the curve for the single torsion angle of 170° and that for a torsion-angle distribution of $\sigma = 16°$ centered at 180°. From this figure, it is found that these curves can be distinguished if the experimental uncertainties are small or the measurements are carried out for longer dephasing times.

**4.11. Comparison with Previous Data.** Various attempts have been made to estimate the amount of aT conformers in semicrystalline PET based on combinations of infrared (IR) and density measurements,[34,39] of IR and DSC measurements,[30,43] of Raman and DSC measurements,[31,38,44] or of IR and X-ray diffraction measurements.[45] Liu and Koenig estimated the aT fraction only by IR spectra using a special algorithm.[35]

According to Lin and Koenig,[34] the aT fraction decreases with increasing degree of crystallinity. Chen et al.[39] also reported a similar tendency for PET polymerized from terephthalic acid. On the other hand, for PET from dimethyl terephthalate, the aT fraction was reported to first increase significantly up to 26% with increasing degree of crystallinity and then decrease gradually.[39] The data by Liu and Koenig gave a similar trend, with the aT fraction first increasing and later decreasing with higher crystallinity; however, the aT fraction was much higher (maximum value of 44%).[35] The reported aT fractions are 3−10%,[34] 6−14%,[39] and 34−40%[35] for samples with degrees of crystallinity in the range of 22−32%. These are for unoriented samples and the degree of crystallinity is controlled by the annealing conditions.

Pastor et al. estimated aT in cPET as almost 0%[31,44] or 2−5%.[38] However, their data appear to be unreliable because the crystalline content estimated from DSC is larger than the trans content from Raman for samples with high degrees of crystallinity. This means that the fraction of cT is larger than the sum fraction of (cT + aT), which is impossible.

Padibjo and Ward[45] and Ajji et al.[30] studied the dependence of the aT fraction on the draw ratio (DR) of oriented PET films. In both cases, the aT fraction was found to increase with increasing DR (up to 48% at DR = 6−7[45] and 20% at DR = 4.8[30]). According to Lu and Hay,[43] the aT fraction depends on the strain rate. For a rate of $17 \times 10^{-3}$ s$^{-1}$, the aT fraction first decreases from 10% to 2−4% at DR = 3.5 and then increases to 18−21% at DR = 5. For the rate of $3.3 \times 10^{-3}$ s$^{-1}$, a similar trend is observed but the change is almost negligibly small. The aT fractions estimated in refs 45, 30, and 43 were 42−48%, 12−20%, and 2−12%, respectively, for samples with degrees of crystallinity in the range of 22−32%.

In summary, there is no agreement in the literature on the relation between cT and aT fractions, and the previously reported aT fractions scatter from 0 to 48% for samples with similar crystallinities of 22−32%. The inconsistency of these previously reported data is probably due to serious problems with the analyses, which are based on indirect difference methods that require assumptions that have not been tested in sufficient detail. Differences in sample synthesis and processing may also play a role. For oriented samples, it has been found that the amorphous component can be oriented and has a substantial degree of order. However, the relation between the aT fraction and the oriented amorphous component is still unclear.

The aT fraction of 20 ± 5% determined in this work is within the wide range of the literature data for similar crystallinity values. Unlike most previous techniques, our approach does not involve the relatively small difference between large trans and crystallinity estimates. Instead, the amorphous trans component is identified directly in terms of its nonideal torsion angle. Knowledge of the aT content is important for the

clarification of the crystallization mechanisms at the very early stages of crystallization.[39] The aT content is also thought to be related to industrially important physical properties of PET, such as transparency.[39]

The aT torsion angle had not been determined experimentally before. Even by our previous static 2D DQ experiments,[1] which gave precise torsion angles for gauche conformers, the difference of cT and aT torsion angles could not be detected. In the CSA-difference-dephasing experiments, the suppression of gauche signals and the high-angular resolution near trans states enable us to detect and quantify aT conformers. This shows that the techniques presented here are especially valuable for conformational analyses of materials whose torsion angles deviate slightly from the ideal trans torsion angle of 180°. Actually, such slight deviations of the torsion angle from the ideal trans state have been observed for a number of polymers even in the crystalline state.[3,46,47]

On the other hand, the high angular resolution near trans is undesirable for experiments aimed at determining small fractions of trans conformers since the non-ideal trans components are partially dephased before the gauche signal components have been completely removed. Nevertheless, the decay constants of gauche and trans components are sufficiently different that a simple deconvolution procedure based on the experimentally determined pure aG line shape yields a good estimate of the total trans content, unless gauche and trans signals completely overlap. In addition, for distinguishing cT and aT components in PET, the measurable decay of the aT component is helpful. For larger torsion angles, 2D DOQSY without MAS provides higher angular resolution, and it also gives more detailed information on torsion-angle distributions.[1,3]

**4.12. Definite Conformational Assignments of CP/MAS Spectra.** The new techniques presented here are useful for the conformational assignment of signals in MAS $^{13}C$ NMR spectra. The CP/MAS experiment is the most standard and easily utilized method in solid-state NMR of polymers. The isotropic chemical shift can be affected by various factors, such as conformation, packing, or hydrogen bonding. While this can provide interesting structural insights, the analysis is often unreliable because the effects of the various factors cannot be separated. The technique presented in this paper can select the information on conformation from among the various effects and can give direct relations between isotropic $^{13}C$ chemical shifts and torsion angles irrespective of the validity of the $\gamma$-gauche effect. Therefore, once the conformational assignments of MAS spectra are carried out by our new ZQ or (DQ-2SQ) techniques, conformations can be easily analyzed by standard MAS spectra without the need for isotopically labeled samples.

**4.13. Comparison of DQ and ZQ Versions.** The sensitivity of the ZQ sequence is reduced by a factor of $1/2^{1/2}$ due to the incomplete conversion of the coherence by the 45° pulses. On the other hand, the chemical-shift recoupling time and the number of 180° pulses is 3-fold reduced compared to the DQ version. Overall, for long chemical-shift recoupling times, the ZQ sequence may become superior, especially for samples with short $^{13}C$ $T_2$ relaxation times. It is an advantage of the (DQ-2SQ) sequence that the minimum DQ excitation and reconversion time can be half of the corresponding ZQ excitation and reconversion times. This produces fewer multiple-spin artifacts in highly labeled samples. Beyond these differences, the data obtained in practice with the two sequences are very similar. For combination with 2D isotropic-chemical-shift correlation, the (DQ-2SQ) version is superior.

**4.14. Advantage over CSA Dephasing Using $^{13}C$ Spin Exchange.** The use of ZQ or DQ states to generate the CSA-difference dephasing is crucial for the experiments discussed here. Even if only isolated $^{13}C$ spin pairs are present in the sample, a simpler spin-exchange (or spin-diffusion) pulse sequence, without a DQ filter, has significant disadvantages. The signal would dephase only to 50%, reducing the dynamic range of the experiment and, more importantly, making it impossible to select trans components because half of the spectral intensity remains in any case. In addition, the natural abundance background is significant even in the 4% $^{13}C-^{13}C$ pair labeled PE sample used here since the ratio of spin pairs and isolated spins is 4.4:1.1. Increasing the labeling level would induce multi-spin interactions, which are quite unfavorable for the present purpose. It should be noted that MQ excitation pulse sequences[23−25] other than HORROR[22] are better for systems with large chemical-shift differences. The incorporation of a ZQ or DQ filter as presented here opens the possibility of characterizing the conformations of various kinds of statistically labeled ordered (crystalline) and disordered (amorphous) materials, including self-assembled monomeric, other polymeric, or biomaterials.

## 5. Conclusions

Two new NMR methods for characterizing the conformations of $^{13}C$-labeled solid polymers under MAS have been presented. By recoupled CSA-difference dephasing of ZQ coherence, or of DQ coherence compensated by evolution of SQ coherence, the relative orientation of two nearby $^{13}C$-labeled sites is measured for each peak in the MAS spectrum. The angular resolution is high for nearly parallel orientations of the chemical-shift tensors, which in particular includes trans conformations involving $CH_2$ groups. For $^{13}CH_2-^{13}CH_2$ groups, the trans peak in the MAS spectrum is selected at long CSA recoupling times, while the initial fast decay identifies a pure gauche MAS line shape. Thus, the dephasing curves for these different line shape components permit measurements of the trans and gauche fractions, possibly in combination with simple deconvolution based on the experimentally measured subspectra. Detailed fits of the dephasing curves provide information on the torsion angles. In amorphous PET, the trans peak in the MAS spectrum has thus been identified for the first time. A (DQ-2SQ)-CSA-filtered 2D INADEQUATE spectrum indicates that, in aPET, the two $CH_2$ groups connected by a trans bond experience similar local fields. In aPET, the dephasing curves obtained after deconvolution yield a trans fraction of 12 ± 3%, with a distribution of torsion angles around 180° and of standard deviation $\sigma = 16°$. In semicrystalline PET, the total trans fraction is 43 ± 3%, the crystallinity 23 ± 5%, and the aT fraction 20 ± 5%, which corresponds to 26% of the noncrystalline component.

**Acknowledgment.** The authors thank Dr. Nicholas Zumbulyadis for providing the $^{13}C$-labeled PET material. We also thank Dr. E. R. deAzevedo and Professor T. J. Bonagamba for making a CODEX FORTRAN simulation program available. H.K. would like to thank

the Ministry of Education, Science, Sports and Culture, Japan, for financial support from a Grant-in-Aid for Encouragement of Young Scientists (Grant 13750830). We also acknowledge partial support of this work by the Director for Energy Research, Office of Basic Energy Science, in the Materials Chemistry Program of Ames Laboratory, operated for the U.S. Department of Energy by Iowa State University (Contract W-7405-Eng-82).

## 6. Appendix

This Appendix describes the effect of the (DQ-2SQ) and ZQ pulse sequences on the state of the spin system, represented by the density operator $\rho(t)$. It evolves under dipolar and chemical-shift interactions as well as radio frequency pulses.[18] While magnetization corresponds to individual spin operators $S_\alpha$ or $L_\beta$, double- or zero-quantum coherences correspond to specific combinations of transverse $S_{x/y}L_{x/y}$ product operators, which evolve with the sum (DQ) or difference (ZQ) of the $S$- and $L$-spin anisotropic chemical shifts. We start out with the calculation of the average Hamiltonians of the two versions of HORROR[22] used.

**6.1. Average Hamiltonian of HORROR in Cartesian Notation.** For the recoupling of the $^{13}C-^{13}C$ dipolar coupling, we use the HORROR nutation pulse,[22] which works well under fast MAS for the small chemical-shift offsets and anisotropies of $CH_2$ groups. Under $^1H$ decoupling and MAS, the $^{13}C-^{13}C$ homonuclear dipolar Hamiltonian during $^{13}C$ nutation in the corresponding interaction frame is described by

$$H_{SL}(t) = \omega_{SL}(t)\left\{3\left(S_z\cos\frac{\omega_r t}{2} \pm S_y \sin\frac{\omega_r t}{2}\right)\left(L_z\cos\frac{\omega_r t}{2} \pm L_y \sin\frac{\omega_r t}{2}\right) - \vec{S}\cdot\vec{L}\right\} \quad \text{(A1)}$$

where the nutation frequency has been set to equal half the MAS rotation frequency, $\omega_r$. The $\pm$ sign corresponds to forward and backward nutations in successive periods of $2t_r$ each, as shown in Figure 2b. The time dependence of the orientation-dependent frequency under MAS in eq A1 is given by

$$\omega_{SL}(t) = \tilde{C}_1\cos(\omega_r t) + \tilde{S}_1\sin(\omega_r t) \quad \text{(A2)}$$

where the $\tilde{C}_1$ and $\tilde{S}_1$ coefficients can be rewritten as $\tilde{C}_1 = C_1\cos\gamma$ and $\tilde{S}_1 = -C_1\sin\gamma$ with

$$C_1 = \frac{\mu_0}{4\pi}\hbar\frac{{\gamma_C}^2}{{r_{SL}}^3}\sqrt{2}\frac{1}{2}\sin 2\beta \quad \text{(A3)}$$

for a two-spin dipolar coupling ($\eta = 0$) with an internuclear distance $r_{SL}$ and gyromagnetic ratio $\gamma_C$. The polar angles ($\beta$, $\gamma$) denote the direction of the $^{13}C-^{13}C$ internuclear vector in the rotor frame (RF) where $Z_{RF}$ is along the rotor axis. The time average of the dipolar interaction, which is doubly time-dependent according to eqs A1 and A2, over periods of $2mt_r$ is[18,25]

$$\begin{aligned}\bar{H}_{SL} &= \frac{1}{2t_r}\int_0^{2t_r} H_{SL}(t)\,dt \\ &= \frac{3}{4}\{\tilde{C}_1(S_zL_z - S_yL_y) \pm \tilde{S}_1(S_yL_z + S_zL_y)\} \\ &= \frac{3}{4}C_1\{(S_zL_z - S_yL_y)\cos\gamma \pm (S_yL_z + S_zL_y)\sin\gamma\}\end{aligned} \quad \text{(A4)}$$

DQ and ZQ coherences can be generated by this average Hamiltonian followed by a suitable 90° or 45° pulse, as shown below. The suppression of the second $\tilde{S}_1$ (or sin $\gamma$) term by + and − sign cancellation when the two alternatives in eq A4 are added is crucial for creating ZQ coherence effectively; it is achieved by forward and backward nutations in the HORROR pulse sequence.

**6.2. Density Operator Analysis of the (DQ-2SQ) Sequence.** In the following, we give a brief density-operator description of the experiments, in terms of simple Cartesian product operators.

**(1) DQ Excitation.** Magnetization after CP, $S_x + L_x$, evolves under the average Hamiltonian in eq A4 with the positive sign. This is found to correspond to precession around an effective fictitious field along the (0, cos $\gamma$, sin $\gamma$) direction in a two-spin space of $J_x = {}^1/_2\,(S_x + L_x)$, $J_y = S_yL_y - S_zL_z$, and $J_z = S_yL_z + S_zL_y$ for a period of $k2t_r$. This is followed by a $90°_{-y}$ pulse so that DQ coherence is generated:

$$\begin{aligned}\text{DQ excitation: } S_x + L_x &\xrightarrow{\bar{H}_{SL}\text{ (weak field along } y)} \\ &2\{(S_zL_z - S_yL_y)\sin\gamma + (S_yL_z + S_zL_y)\cos\gamma\}\sin\phi_{SL} \\ &\xrightarrow{90°_{-y}} 2\{(S_xL_x - S_yL_y)\sin\gamma + (S_yL_x + S_xL_y)\cos\gamma\}\sin\phi_{SL}\end{aligned} \quad \text{(A5)}$$

where $\phi_{SL} = {}^3/_4C_1k2t_r$ according to eq A4. In our experiments, we used $k = 1$. Here and in the following, for the sake of brevity only the relevant terms of the density operator have been retained.

**(2) Recoupled CSA Evolution of DQ Coherence.** The DQ coherence thus obtained evolves for $2nt_r$ under the CSA that is recoupled by 180° pulses spaced by $t_r/2$ as in CODEX[26,27]

$$\begin{aligned}&2\{(S_xL_x - S_yL_y)\sin\gamma + (S_yL_x + S_xL_y)\cos\gamma\}\sin\phi_{SL} \\ &\xrightarrow{\text{DQ-CSA evolution}} 2\{(S_xL_x - S_yL_y)\sin\gamma + (S_yL_x + S_xL_y)\cos\gamma\}\sin\phi_{SL}\cos\Phi_\Sigma + 2\{(S_xL_x - S_yL_y)\cos\gamma + (S_yL_x + S_xL_y)\sin\gamma\}\sin\phi_{SL}\sin\Phi_\Sigma\end{aligned} \quad \text{(A6)}$$

Here, the phase acquired under the influence of the recoupled CSA sum frequency is $\Phi_\Sigma = \Phi_S + \Phi_L$.

**(3) DQ Reconversion.** After DQ evolution, the sin $\phi_{SL}$ cos $\Phi_\Sigma$ term of the DQ coherence in eq A6 is reconverted to SQ coherence by a $90°_x$ pulse and then to magnetization as follows:

$$\begin{aligned}&2\{(S_xL_x - S_yL_y)\sin\gamma + (S_yL_x + S_xL_y)\cos\gamma\} \\ &\sin\phi_{SL}\cos\Phi_\Sigma \xrightarrow{90°_{+x}} 2\{(S_xL_x - S_zL_z)\sin\gamma \\ &- (S_zL_x + S_xL_z)\cos\gamma\}\sin\phi_{SL}\cos\Phi_\Sigma \\ &\xrightarrow{\bar{H}_{SL}\text{ (weak field along } y)} - \\ &(S_y + L_y)\sin^2\phi_{SL}\cos\Phi_\Sigma\end{aligned} \quad \text{(A7)}$$

The sin $\phi_{SL}$ sin $\Phi_\Sigma$ term of eq A6 is correspondingly reconverted after a 90° pulse with a nonquadrature phase of $1/2^{1/2}(x + y)$ and $\bar{H}_{SL}$ under a weak field along the $1/2^{1/2}$ $(-x + y)$ direction.

**(4) Matched CSA Evolution of SQ Coherence.** The reconverted magnetization (i.e., observable SQ coherence) evolves further under the recoupled CSA. To compensate the doubled phase acquired in the DQ evolution period, the total duration of the SQ-evolution period is twice as long as that of DQ evolution, that is,

$4nt_r$, as shown in Figure 2a. By combining cosine and sine components obtained as described in the preceding paragraph, we arrive at the following final formula:

$$\begin{aligned}\cos\Phi_\Sigma \sin^2\phi_{SL}\{\exp(i2\Phi_S) + \exp(i2\Phi_L)\} - \\ i\sin\Phi_\Sigma \sin^2\phi_{SL}\{\exp(i2\Phi_S) + \exp(i2\Phi_L)\} = \\ [\exp\{+i\Phi_\Delta\} + \exp\{-i\Phi_\Delta\}]\sin^2\phi_{SL} = \\ 2\cos\Phi_\Delta \sin^2\phi_{SL} \quad \text{(A8)}\end{aligned}$$

Here, $\Phi_\Delta = \Phi_S - \Phi_L$ is the phase acquired under the chemical-shift anisotropy difference of $S$ and $L$, similar to that in CODEX.[26,27]

**6.3. Density Operator Analysis of the ZQ Sequence. (1) ZQ Excitation.** The magnetization after CP, $S_x + L_x$, evolves for $k'2t_r$ under the average dipolar Hamiltonian $\bar{H}_{SL} = 0.75\tilde{C}_1(S_zL_z - S_yL_y)$, followed by a $45°_{-x}$ pulse and a $z$-filter so that ZQ coherence is generated:

$$\begin{aligned}&\text{ZQ excitation: } S_x + L_x \xrightarrow{\bar{H}_{SL}} 2(S_yL_z + S_zL_y)\sin\phi'_{SL} \\ &\xrightarrow{45°_{-x}} 2(S_yL_y - S_zL_z)\sin\phi'_{SL} \xrightarrow{\text{z-filter}} -2S_zL_z\sin\phi'_{SL} \\ &\begin{cases}\xrightarrow{90°_{\pm x}} -2S_yL_y\sin\phi'_{SL} \\ \xrightarrow{90°_{\pm y}} -2S_xL_x\sin\phi'_{SL}\end{cases} \quad \text{(A9)}\end{aligned}$$

where $\phi'_{SL} = {}^3/_4C_1(\cos\gamma)k'2t_r$. Note that a less favorable $\gamma$-dependent modulation of the $S_zL_z$ term was avoided by using the $\bar{H}_{SL} = 0.75\tilde{C}_1(S_zL_z - S_yL_y)$ HORROR average dipolar Hamiltonian, cf. eq A4, obtained by alternating the phases of the 360° nutation pulses. This is also indicated in Figure 2b. Note also that to complete one phase alternation, $k' = 2$ is required.

The summation of coherence generated by the final $90°_x$ and $90°_y$ pulses in eq A9 creates pure ZQ coherence, $-2(S_xL_x + S_yL_y)\sin\phi'_{SL}$. Phase alternation, for instance between $90°_x$ and $90°_{-x}$, leaves the bilinear coherences invariant while suppressing $z$ polarization:

$$I_z \xrightarrow{90°_{\pm x}} \pm I_y$$

**(2) Recoupled CSA Evolution of ZQ Coherence.** The ZQ coherence thus obtained evolves for a time $2nt_r$ under the recoupled chemical-shift-anisotropy difference Hamiltonian, acquiring a phase $\Phi_\Delta$:

$$\begin{aligned}-2(S_xL_x + S_yL_y)\sin\phi'_{SL} \xrightarrow{\text{ZQ−CSA evolution}} -2\{(S_xL_x + \\ S_yL_y)\cos\Phi_\Delta - (S_xL_y - S_yL_x)\sin\Phi_\Delta\}\sin\phi'_{SL} \quad \text{(A10)}\end{aligned}$$

**(3) ZQ Reconversion.** After ZQ evolution, the ZQ coherence is reconverted to SQ magnetization as follows:

$$\begin{aligned}-2\{(S_xL_x + S_yL_y)\cos\Phi_\Delta - (S_xL_y - S_yL_x)\sin\Phi_\Delta\} \\ \sin\phi'_{SL} \xrightarrow{90°_{+y}} -2\{(S_zL_z + S_yL_y)\cos\Phi_\Delta \\ - (S_zL_y - S_yL_z)\sin\Phi_\Delta\}\sin\phi'_{SL} \\ \xrightarrow{\text{z-filter}} -2S_zL_z\cos\Phi_\Delta\sin\phi'_{SL} \\ \xrightarrow{45°_{-x}} -\{(S_zL_z + S_yL_y) - (S_yL_z + S_zL_y)\} \\ \cos\Phi_\Delta\sin\phi'_{SL} \xrightarrow{\bar{H}_{SL}} (S_x + L_x)\cos\Phi_\Delta\sin^2\phi'_{SL} \quad \text{(A11)}\end{aligned}$$

Note that according to eq A9, two scans are required to generate this signal. This reduces the sensitivity per unit time by a factor of $1/2^{1/2}$ compared to the (DQ-2SQ) version of the experiment.

## References and Notes


(1) Schmidt-Rohr, K.; Hu, W.; Zumbulyadis, N. *Science* **1998**, *280*, 714.
(2) Kaji, H.; Schmidt-Rohr, K. *Macromolecules* **2000**, *33*, 5169.
(3) Kaji, H.; Schmidt-Rohr, K. *Macromolecules* **2001**, *34*, 7368.
(4) Kaji, H.; Schmidt-Rohr, K. *Macromolecules* **2001**, *34*, 7382.
(5) Tonelli, A. E. *NMR Spectroscopy and Polymer Microstructure: The Conformational Connection*; VCH Publishers: New York, 1989.
(6) Bunn, A.; Cudby, M. E. A.; Harris, R. K.; Packer, K. J.; Say, B. J. *J. Chem. Soc., Chem. Commun.* **1981**, 15.
(7) Ando, I.; Kameda, T.; Asakawa, N. In *Solid State NMR of Polymers*; Ando, I., Asakura, T., Eds.; Elsevier: New York, 1998; pp 819−852.
(8) Asakura, T.; Demura, M.; Nishikawa, N.; Yoshimizu, H. In *Solid State NMR of Polymers*; Ando, I., Asakura, T., Eds.; Elsevier: New York, 1998; pp 853−890.
(9) Asakura, T.; Iwadate, M.; Demura, M.; Williamson, M. P. *Int. J. Biol. Macromol.* **1999**, *24*, 167.
(10) Saito, H.; Tabeta, R.; Shoji, A.; Ozaki, T.; Ando, I. *Macromolecules* **1983**, *16*, 1050.
(11) Born, R.; Spiess, H. W. *Ab initio Calculations of Conformational Effects on $^{13}C$ NMR Spectra of Amorphous Polymers*; Spring-Verlag: Berlin, 1997; Vol. 35.
(12) Schilling, F. C.; Tonelli, A. E.; Cholli, A. L. *J. Polym. Sci. B: Polym. Phys.* **1992**, *30*, 91.
(13) VanderHart, D. L. *J. Magn. Reson.* **1981**, *44*, 117.
(14) Muller, L. *J. Magn. Reson.* **1984**, *59*, 326.
(15) Bax, A.; Freeman, R. *J. Magn. Reson.* **1980**, *41*, 507.
(16) Ishii, Y.; Ashida, J.; Terao, T. *Chem. Phys. Lett.* **1995**, *246*, 439.
(17) Bennett, A. E.; Rienstra, C. M.; Auger, M.; Lakshmi, K. V.; Griffin, R. G. *J. Chem. Phys.* **1995**, *103*, 6951.
(18) Schmidt-Rohr, K.; Spiess, H. W. *Multidimensional Solid-State NMR and Polymers*; Academic Press: London, 1994.
(19) Schmidt-Rohr, K. *Macromolecules* **1996**, *29*, 3975.
(20) Ernst, R. R.; Bodenhausen, G.; Wokaun, A. *Principles of Nuclear Magnetic Resonance in One and Two Dimensions*; Clarendon Press: Oxford, 1987.
(21) Gullion, T.; Schaefer, J. *J. Magn. Reson.* **1989**, *81*, 196.
(22) Nielsen, N. C.; Bildsøe, H.; Jakobsen, H. J.; Levitt, M. H. *J. Chem. Phys.* **1994**, *101*, 1805.
(23) Lee, Y. K.; Kurur, N. D.; Helmle, M.; Johannessen, O. G.; Nielsen, N. C.; Levitt, M. H. *Chem. Phys. Lett.* **1995**, *242*, 304.
(24) Hohwy, M.; Jakobsen, H. J.; Edén, M.; Levitt, M. H.; Nielsen, N. C. *J. Chem. Phys.* **1998**, *108*, 2686.
(25) Sun, B.-Q.; Costa, P. R.; Kocisko, D.; Lansbury, P. T., Jr.; Griffin, R. G. *J. Chem. Phys.* **1995**, *102*, 702.
(26) deAzevedo, E. R.; Hu, W.-G.; Bonagamba, T. J.; Schmidt-Rohr, K. *J. Am. Chem. Soc.* **1999**, *121*, 8411.
(27) deAzevedo, E. R.; Hu, W.-G.; Bonagamba, T. J.; Schmidt-Rohr, K. *J. Chem. Phys.* **2000**, *112*, 8988.
(28) Sefcik, M. D.; Schaefer, J.; Stejskal, E. O.; McKay, R. A. *Macromolecules* **1980**, *13*, 1132.
(29) Gabrielse, W.; Gaur, H. A.; Feyen, F. C.; Veeman, W. S. *Macromolecules* **1994**, *27*, 5811.
(30) Ajji, A.; Guevremont, J.; Cole, K. C.; Dumoulin, M. M. *Polymer* **1996**, *37*, 3707.
(31) Rodriguez-Cabello, J. C.; Quintanilla, L.; Pastor, J. M. *J. Raman Spectrosc.* **1994**, *25*, 335.
(32) Yazdanian, M.; Ward, I. M.; Brody, H. *Polymer* **1985**, *26*, 1779.
(33) Cunningham, A.; Ward, I. M.; Willis, H. A.; Zichy, V. *Polymer* **1974**, *15*, 749.
(34) Lin, S. B.; Koenig, J. L. *J. Polym. Sci. Polym. Phys. Ed.* **1982**, *20*, 2277.
(35) Liu, J.; Koenig, J. L. *Anal. Chem.* **1987**, *59*, 2609.
(36) A slightly faster $T_{1\rho}$ decay has been observed for the amorphous component in cPET, compared to the crystalline component, during the CP time of 0.5 ms. This results in a relative intensity attenuation of the amorphous signal by 0.88. Corrections by this factor are not reflected in the plotted data, but have been applied to the final composition data.
(37) In the quantitative data analysis of the cPET spectra, it must be taken into account that the $S_0$ spectra of Figure 5 show

preferential $T_2$ decay of the amorphous signals. In other words, at the larger $n$ values, the gauche components are visibly under-represented because their signal decayed preferentially during the ZQ evolution. On the basis of the pure-gauche signal $\Delta S$ for $n = 1$, the preferential-dephasing factors were estimated, and the signal fractions in the $S(n)$ spectra were correspondingly corrected on the basis of the approximate 60:40 G:T composition. For instance, the gauche component was most strongly under-represented at $n = 4$, by 18%, and the area $S_0$ of the reference spectrum was therefore corrected by (0.6 * 1.18 + 0.4) = 1.11. The trans component of $S$ must be reduced by this factor, the gauche component increased by 1.18/1.11. The uncertainties of the correction procedure have been taken into account in the error analysis; the uncorrected values are all within the error margins shown. The same approach had also been applied to the aPET data shown above, but there the corrections were <1% of the total area $S_0$, i.e., clearly within the error margins from other uncertainties. This correction was applied to the data before plotting.

(38) Fernandez, M. R.; Merino, J. C.; Pastor, J. M. *Polym. Eng. Sci.* **2000**, *40*, 95.
(39) Chen, W.; Jofgren, E. A.; Jabarin, S. A. *J. Appl. Polym. Sci.* **1998**, *70*, 1965.
(40) Murthy, N. S.; Zero, K.; Minor, H. *Macromolecules* **1994**, *27*, 1484.
(41) Murthy, N. S.; Minor, H.; Bednarczyk, C.; Krimm, S. *Macromolecules* **1993**, *26*, 1712.
(42) Murthy, N. S.; Correale, S. T.; Minor, H. *Macromolecules* **1991**, *24*, 1185.
(43) Lu, X. F.; Hay, J. N. *Polymer* **2001**, *42*, 8055.
(44) Quintanilla, L.; Rodriguez-Cabello, J. C.; Jawhari, T.; Pastor, J. M. *Polymer* **1993**, *34*, 3787.
(45) Padibjo, S. R.; Ward, I. M. *Polymer* **1983**, *24*, 1103.
(46) Tadokoro, H. *Structure of Crystalline Polymers*; J. Wiley & Sons: New York, 1979.
(47) Kaji, H.; Horii, F. *Macromolecules* **1997**, *30*, 5791.

MA020246J